

Equilibrium thermodynamic properties of interacting two-component bosons in one dimension

Antoine Klauser^{1,2} and Jean-Sébastien Caux²

¹*Instituut-Lorentz, Universiteit Leiden, P. O. Box 9506, 2300 RA Leiden, The Netherlands and*

²*Institute for Theoretical Physics, Universiteit van Amsterdam, 1018 XE Amsterdam, The Netherlands*

(Dated: September 25, 2021)

The interplay of quantum statistics, interactions and temperature is studied within the framework of the bosonic two-component theory with repulsive delta-function interaction in one dimension. We numerically solve the thermodynamic Bethe Ansatz and obtain the equation of state as a function of temperature and of the interaction strength, the relative chemical potential and either the total chemical potential or a fixed number of particles, allowing to quantify the full crossover behaviour of the system between its low-temperature ferromagnetic and high-temperature unpolarized regime, and from the low coupling decoherent regime to the fermionization regime at high interaction.

I. INTRODUCTION

The increasingly common experimental realization of interacting quantum systems using cold atoms has recently reignited interest in pushing our understanding of many-body physics beyond the traditional mean-field level [1]. This aspect is most in prominence in effectively one-dimensional realizations of bosonic ⁸⁷Rb quantum gases with tunable interaction strength [2–6], for which the whole crossover from weakly- to strongly-interacting physics is accessible.

The case of locally interacting atoms confined to a uniform one-dimensional channel has the theoretical peculiarity of being integrable. The simplest case of a single bosonic species defines the well-known Lieb-Liniger model [7, 8] for which a recent experimental study has shown that the observed thermodynamic properties can be understood from the theory of integrable systems at finite temperatures [9]. In order to study even richer highly correlated systems, multicomponent (spinor) gases have been experimentally realized [10–12]. This extension involves different hyperfine states which provide a pseudospin degree of freedom [13–16]. The control of the intra- and inter-species interaction strength via Feshbach resonances or state-dependent potentials [17–19] opens the way for realizing a variety of integrable models.

The main interest in pursuing the study of multicomponent systems is that they provide situations where important interaction and quantum statistics effects coexist. These two aspects are not unrelated even in single-component systems: as a simple illustration, for a single bosonic species in one dimension, the limit of infinitely strong interactions (impenetrable bosons) causes a crossover from bosonic to effectively fermionic behaviour [20, 21], at least for physical quantities of density type. Considering more than one component however opens the door to much richer effects like the presence of spin wave excitations, with the possibility of crossover to many more regimes than the one component case.

The study of multicomponent integrable systems really begins with the spin-1/2 fermion problem [22–26]. An interesting feature of this system is that the attrac-

tive case has a correspondence to a bosonic system with twice the interaction, in the sense that the equation for the ground state and particle energy coincide up to a sign [26]. A fundamental step forward was thereafter achieved by Yang, who showed that the repulsive delta-function interaction problem admitted an exact solution irrespective of the symmetry requirement imposed on the wavefunction [27]. For spin-1/2 particles, he showed that a generalized Bethe hypothesis in the form of what is today called a nested Bethe ansatz could provide the system's wavefunctions, obtained the continuum equations for the ground state, and calculated the general bound-state S -matrices [28]. Sutherland [29] generalized this to any irreducible representation of the permutation group, so that in particular systems of type (in his notation) $B^x F^y$ with x species of bosons and y species of fermions were amenable to an exact solution [30]. The ground state and excitations of multicomponent fermionic system were studied, both for repulsive and attractive interactions, by Schlottmann [31, 32]. This made extensive use of the ‘string hypothesis’ for the solutions to the Bethe equations, yielding the various dispersion branches in the repulsive case, and the gapped color singlet ground states in the attractive one.

The bosonic multicomponent case has been less extensively studied. For two components and in contrast with the Fermi gas, the ground state is (pseudospin) polarized as expected from basic arguments [30] or more formally from a general theorem valid when spin-dependent forces are absent [33]. In pseudospin language, the ground state is thus ferromagnetic, and the excitations at large coupling correspond to those in an isotropic XXX ferromagnetic chain [34], revealing thermodynamic properties which are drastically different from those of the one-component Lieb-Liniger gas [35, 36]. Furthermore, recent studies of the ferromagnetic ground state revealed different dispersions for the charge and pseudospin excitations which therefore exhibits a spin-charge separation [37, 38]. The regime of strong interaction is still not completely understood and even if Girardeau's Fermi-Bose mapping has been showed and used for the study of the 1D spinor Bose gases [39] leading to a paramagnetic

Tonk-Girardeau regime [34], this approach fails to provide first correction terms to this fermionization regime since the discernability of the bosons is missing.

The purpose of our paper is to further stimulate the contact between integrability theory and experiments on multicomponent cold atoms, by providing quantitative predictions for the equation of state and population densities of two-component interacting Bose gases as a function of temperature, interaction strength and of either the available chemical potentials or the chemical potential difference and a fixed density of particles. This work broadens and extends our earlier paper [40]. The paper is organized as follows. In section II, after defining our notations, we quickly review the construction of the eigenstates of the theory using the Bethe Ansatz, and how these can be used to obtain the thermodynamics of the system in the continuum limit via the solution of a (infinite) set of coupled integral equations. Section III outlines the method we have used to solve this system numerically, using two different approaches allowing cross-checking of the results. Section IV discusses the effect of the thermal fluctuation over the ferromagnetic ground-state, whereas section V provides results on the more challenging intermediate regimes. Section VI discusses the results in the decoherents regime of low coupling where we compare the numerical results with a perturbative result and section VII presents the results at strong coupling where the gas enters the fermionization regime. We end with conclusions and perspectives.

II. SETUP

Consider a collection of bosonic atoms of equal mass but having an internal $SU(2)$ degree of freedom (in practice, this would be for example two distinguishable hyperfine states, and could be thought of as a (pseudo-)spin- $1/2$). The unique feature differentiating from a single species is the fact that distinguishability imposes symmetry of the many-particle wavefunction on the same-spin particles only. For definiteness, we consider a one-dimensional ring of length L , in which a total of N atoms circulate. The first-quantized Hamiltonian of the system includes a free dynamical term to which a spin-blind interaction term is added, and reads

$$\mathcal{H}_N = -\frac{\hbar^2}{2m} \sum_{i=1}^N \frac{\partial^2}{\partial x_i^2} + g_{1D} \sum_{1 \leq i < j \leq N} \delta(x_i - x_j). \quad (1)$$

The effective one-dimensional coupling parameter g_{1D} is related to the effective 1D scattering length a_{1D} [41] via the relation $g_{1D} = \hbar^2 a_{1D} / 2m$. Hereafter, we will use the effective interaction parameter $c = g_{1D} m / \hbar^2$, and adopt the traditional convention of setting $\hbar = 2m = 1$ to simplify the notations. Note that this choice of interaction term involves fine-tuning two parameters: more generally, we could have different intra- and inter-species scattering lengths. To preserve integrability however, these

must all be equal.

Specializing to N atoms of which M have (in the adopted cataloguing) spin down, the Bethe Ansatz provides eigenfunctions fully characterized by sets of rapidities (quasi-momenta) k_j , $j = 1, \dots, N$ and pseudospin rapidities λ_α , $\alpha = 1, \dots, M$, provided these obey the $N + M$ coupled equations [27, 29]

$$\begin{aligned} e^{ik_j L} &= - \prod_{l=1}^N \frac{k_j - k_l + ic}{k_j - k_l - ic} \prod_{\alpha=1}^M \frac{k_j - \lambda_\alpha - \frac{ic}{2}}{k_j - \lambda_\alpha + \frac{ic}{2}}, \\ \prod_{l=1}^N \frac{\lambda_\alpha - k_l - \frac{ic}{2}}{\lambda_\alpha - k_l + \frac{ic}{2}} &= - \prod_{\beta=1}^M \frac{\lambda_\alpha - \lambda_\beta - ic}{\lambda_\alpha - \lambda_\beta + ic}, \end{aligned} \quad (2)$$

for $j = 1, \dots, N$ and $\alpha = 1, \dots, M$. For a generic eigenstate, the solution to the Bethe equations is rather involved and cannot be obtained in closed form. Two observations allow to push the treatment further: first, for $c > 0$, the k_j rapidities live on the real axis. This is not true of the λ_α which are found to be generically complex, but arranged into regular patterns called strings [42, 43]. An n -string of λ 's is a congregation of n rapidities sharing the same real value and having an even spacing of height c in the imaginary direction. The adopted notation for the a -th member of a n -string labeled by the index α and centered on Λ_α^n is thus $\lambda_\alpha^{n,a} = \Lambda_\alpha^n + i\frac{c}{2}(n+1-2a)$, with the equality being exact only up to deviations which (according to the traditional string hypothesis) vanish in the infinite size limit. Throughout our work, we will adopt this as a working hypothesis. Since the total number of each type of string is conserved under time evolution, each string type represents a quasiparticle of the theory. In the thermodynamic limit, the distribution of all rapidities can be encoded into a set of smooth functions representing the densities of roots for each string type. The Bethe equations then become a set of coupled integral equations for (quasi)particle and (quasi)hole root distribution functions. We refer the reader who is unfamiliar with these to our summary of important formulas in appendix (A).

The Thermodynamic Bethe Ansatz (TBA) allows to exploit the condition of thermal equilibrium [44, 45] to obtain the Yang-Yang-Takahashi (YYT) like equations [34, 35, 45] for $\epsilon(\lambda)$, the dressed energy, and $\epsilon_n(k)$, length- n string dressed energy, $n = 1, 2, \dots$

$$\begin{aligned} \epsilon(k) &= k^2 - \mu - \Omega - T a_2 * \ln \left[1 + e^{-\epsilon(k)/T} \right] \\ &\quad - T \sum_{n=1}^{\infty} a_n * \ln \left[1 + e^{-\epsilon_n(k)/T} \right] \\ \frac{\epsilon_1(k)}{T} &= f * \ln \left[1 + e^{-\epsilon(k)/T} \right] + f * \ln \left[1 + e^{\epsilon_2(k)/T} \right], \\ \frac{\epsilon_n(k)}{T} &= f * \ln \left[1 + e^{\epsilon_{n+1}(k)/T} \right] + f * \ln \left[1 + e^{\epsilon_{n-1}(k)/T} \right] \\ &\quad (n > 1), \end{aligned} \quad (3)$$

with the standard convolution notation $g * h(k) \equiv \int_{-\infty}^{\infty} dk' g(k - k') h(k')$, and the kernels $a_n(k) \equiv$

$\frac{1}{\pi} \frac{nc/2}{(nc/2)^2 + k^2}$ and $f(k) = \frac{1/2c}{\cosh(\pi k/c)}$. The set of coupled equations is completed with the asymptotic conditions

$$\lim_{n \rightarrow \infty} \frac{\varepsilon_n(k)}{n} = 2\Omega \quad (4)$$

for high-level functions. From these can be derived the large-rapidity asymptotes

$$\lim_{k \rightarrow \infty} \varepsilon_n(k) \equiv \varepsilon_n^\infty, \quad n = 1, 2, \dots \quad (5)$$

for the large rapidity asymptotic values of the individual functions, where we have defined the numbers

$$\varepsilon_n^\infty \equiv 2\Omega n + T \ln \left(\left(\frac{1 - e^{-\frac{2\Omega}{T}(n+1)}}{1 - e^{-\frac{2\Omega}{T}n}} \right)^2 - e^{-\frac{2\Omega}{T}n} \right) \quad (6)$$

The thermodynamics of the system is provided by the solution set of dressed energies as a function of the temperature T , the total $\mu (= \frac{\mu_1 + \mu_2}{2}$ with μ_i the chemical potential specific to the i th component) and relative $\Omega (= \frac{\mu_1 - \mu_2}{2})$ chemical potential (see appendix C concerning the c parameter). The Gibbs free energy per unit length is given by

$$g = -\frac{T}{2\pi} \int_{-\infty}^{\infty} \ln \left[1 + e^{-\varepsilon(k)/T} \right] dk \quad (7)$$

while the linear density of the i th boson component is

$$n_i = -\frac{1}{2} \left(\frac{\partial g}{\partial \mu} + (-1)^{i-1} \frac{\partial g}{\partial \Omega} \right) \quad (8)$$

The entropy density is given by the standard thermodynamic identity

$$s = -\frac{\partial g}{\partial T} \quad (9)$$

and the local density-density correlator [46, 47] is given (using the Hellman-Feynman theorem) by

$$g^{(2)} = \frac{\sum_{i,j} \langle \Psi_i^\dagger \Psi_j^\dagger \Psi_j \Psi_i \rangle}{(\sum_i \langle \Psi_i^\dagger \Psi_i \rangle)^2} = \frac{-\frac{\partial g}{\partial c}}{(\sum_i n_i)^2} \quad (10)$$

III. NUMERICAL TREATMENT

To solve the infinite system of transcendental coupled equations (3), we have developed two different numerical algorithms. We can then independently check the results by comparison. We first discuss the common approach for the numerical treatment. Afterwards, we will describe and motivate the choices we made to build the two algorithms.

Two cutoffs are applied on the system (3) to implement a numerical process. Firstly we reduce the number of functions for computing to n_{\max} , replacing for $n > n_{\max}$ these functions by their asymptotic value (limit $n \rightarrow \infty$

in (4)). Secondly, we reduce the range of integration of the convolution to a finite value. Supposing that as $k \rightarrow \pm\infty$, $\varepsilon(k) \sim k^2$ and that ε_n becomes ε_n^∞ (5), we limit the range of the k values to $[-\Delta_n : \Delta_n]$. In consequence, we estimate the solution by $1+n_{\max}$ functions $\{\varepsilon, \varepsilon_1, \varepsilon_2, \dots, \varepsilon_{n_{\max}}\}$ and we evaluate them by N_i points over the interval $[-\Delta_i : \Delta_i]$ ($i = 0, \dots, n_{\max}$). To compute the solution we proceed by iterations, starting from the free bosons form of ε and the asymptotic values ε_n^∞ .

The previous paragraph describes how to get the particle dressed energy, $\varepsilon(k)$, and consequently allows one to compute the Gibbs free energy (7). But in order to compute any other thermodynamic quantity involving a derivative of g (8, 9, 10), we use the system for the corresponding set of functions $\{\frac{\partial \varepsilon}{\partial var}, \frac{\partial \varepsilon_1}{\partial var}, \dots\}$ with $var \in \{\mu, \Omega, T, c\}$ (B1, B2, B3). We achieve the numerical solutions by the same method of discretisation introduced before and using the set $\{\varepsilon, \varepsilon_1, \dots, \varepsilon_{n_{\max}}\}$ solution of (3). It would be possible to numerically differentiate G or ε to compute these quantities. This method would however achieve only much less accuracy for given computational effort.

1. Fixed density of particles

For physical interpretation of the results and for the identification of the different regime crossovers, results with fixed density of particles could be more convenient. For this purpose, we implemented a Newton's method on top of our main algorithms that finds the chemical potential, μ , corresponding to a desired density, $n_1 + n_2$.

2. Accuracy and precision

By the use of the method mentioned above to solve the system, we are confronted with two limitations on exactitude. The first comes from the numerical approximation of the system: discretization of the functions, limitation of the integration range and the number of function leads to an imprecision on the results. Second, the fact that we solve the system by iteration approaching but not reaching the solution, leads to an inaccuracy.

The imprecision is limited as described hereafter. The discretisation of the functions adds an error $\mathcal{O}(\frac{1}{N^2})$ in the convolutions (N being the numbers of points) which induces an imprecision that one can easily keep low. Concerning the range cutoff, all the thermodynamic quantities are $\propto e^{-\varepsilon(k)/T}$, with $\varepsilon(k) \sim k^2$ when $k \gg 1$. Therefore we reduce this effect on the results by taking an appropriate k spacing such that $\Delta^2/T \gg 1$. Finally, as we can see from (3, B1,B2,B3), all the contributions of the ε_n functions in $\varepsilon(k)$ are $\propto e^{-\varepsilon_n(k)/T}$. Knowing that for $n \gg 1$, $\varepsilon_n(k) \cong 2n\Omega$, we therefore keep this imprecision small by choosing $\frac{n_{\max}\Omega}{T} \gg 1$. In the results shown in all plots, the precision of the results is estimated to always be much smaller than the width of the curves.

The problem is different for the accuracy. Supposing that the solutions $\{\varepsilon, \varepsilon_1, \varepsilon_2, \dots\}$, $\{\frac{\partial \varepsilon}{\partial var}, \frac{\partial \varepsilon_1}{\partial var}, \dots\}$ ($var \in \{\mu, \Omega, T, c\}$) exist, we suppose that by iteration we approach these solutions but the distance from the solution is nevertheless unknown. We estimate the accuracy empirically. Increasing the total number of iterations exponentially, we observe the convergence of the results and judge the accuracy value. In the following results, the accuracy is estimated to be of order of the line width and therefore globally is the higher limitation on exactitude of the results.

A. FFT based algorithm

1. Idea

During the iterative process, the major part of calculation time is taken by the evaluation of each convolution. Indeed by calculating the integrals by simple trapezoidal sums, this charge represents $\sim \mathcal{O}(N_i N_{i\pm 1})$ operations for each function. Starting from this observation, the basic idea of this algorithm is to use

the Fast Fourier Transform to calculate the convolution: $(f * g)(x) = \text{FT}^{-1}(\text{FT}(f) \cdot \text{FT}(g))$ (with FT: Fourier Transform). The computing time of each convolution using FFT is thus only $\sim \mathcal{O}(N_i \log(N_i))$. The conditions of use of the FFT are that the functions f and g must be integrable and that the values of these functions must be zero outside $[-\Delta_i : \Delta_i]$. This could be easily achieved by treating the constant part of the function separately from the nontrivial part. Moreover this method imposes the numerical constraints that all the points must be equally spaced and that the range and the numbers of points of each function must be the same.

2. Practically

As a consequence of this, we have a set of $n_{\max} + 1$ functions each to be evaluated on N points and within the range $[-\Delta, \Delta]$. We start by setting up the system with three arbitrary parameters: $(D_0, \Delta_0, n_{\max}^0)$ with $D = \frac{N}{2\Delta}$. During the convergence, we adjust them dynamically with the use of the following precision indicators. We firstly estimate the n th iteration precision with

$$\sigma_{\text{it}} = -\frac{T}{2\pi G} \frac{2\Delta}{N} \sum_{i=1}^N \left| \ln \left[1 + \exp\left(-\frac{\varepsilon^{(n)}(k_i)}{T}\right) \right] - \ln \left[1 + \exp\left(-\frac{\varepsilon^{(n-1)}(k_i)}{T}\right) \right] \right| \quad (11)$$

with $\varepsilon^{(n)}(k_i)$ being the value of $\varepsilon(k_i)$ after n iterations. This formula has to be understood as the variation of the Gibbs free energy between two steps (see (7)). We measure similarly how the parameters n_{\max} and Δ influence the precision with these two indicators

$$\sigma_{n_{\max}} = -\frac{T}{2\pi G} \frac{2\Delta}{N} \sum_{i=1}^N \left| \ln \left[1 + \exp\left(-\frac{\varepsilon_{n_{\max}}(k_i)}{T}\right) \right] - \ln \left[1 + \exp\left(-\frac{\varepsilon_{n \rightarrow \infty}}{T}\right) \right] \right| \quad (12)$$

$$\sigma_{\Delta} = -\frac{T2\Delta}{2\pi n_{\max} G} \sum_n \left| \frac{1}{2} \ln \left[\left(1 + \exp\left(-\frac{\varepsilon_n(k_1)}{T}\right) \right) \left(1 + \exp\left(-\frac{\varepsilon_n(k_N)}{T}\right) \right) \right] - \ln \left[1 + \exp\left(-\frac{\varepsilon_n^{\infty}}{T}\right) \right] \right| \quad (13)$$

During computation, if $\sigma_{n_{\max}} > \sigma_{\text{it}}$, n_{\max} is increased and if $\sigma_{\Delta} > \sigma_{\text{it}}$, Δ is lengthened. The precision related by the density of points, D , is hard to quantify but can be estimated by cross-checking with the second method which has a non-uniform distribution of points. We then increase it step by step as one goes along the iterating process.

Once satisfactory values for $\sigma_{\text{it}}^{\text{sol}}, D^{\text{sol}}$ are achieved, we assume the solution has been reached and we calculate the Gibbs free energy from (7). The derivatives of the Gibbs free energy are computed using the derivative systems (B1, B2, B3) with the final $(\Delta, n_{\max}, D^{\text{sol}})$ determined by the first iterative process and we approximate

the precision during the iterations by

$$\sigma_{\text{it}}^{\text{var}} = \frac{1}{2\pi \frac{\partial G}{\partial var}} \sum_{i=1}^N \Delta_k \frac{\left| \frac{\partial \varepsilon(k_i)^n}{\partial var} - \frac{\partial \varepsilon(k_i)^{n-1}}{\partial var} \right|}{1 + \exp\left(\frac{\varepsilon(k_i)^n}{T}\right)}, \quad var \in \{\mu, \Omega, T, c\}. \quad (14)$$

Since the arbitrary $\sigma_{\text{it}}^{\text{var, sol}}$ with D^{sol} are reached, we consider that we have a good evaluation of the solutions.

B. Flexible-density method

A second, completely independent implementation of the numerical solution to the coupled integral equations has been pursued as part of our work. Here, we do not

make use of the fast Fourier transform, but rather maintain total flexibility in the choice 1) of density of sampling points within each function, 2) of the Δ_i limits used at each level, 3) of the relative total number of points used at each level, and 4) of the total number of functions used. This advantage allows one to concentrate computational resources where they are needed, but comes at the cost of being only able to perform convolutions between *e.g.* levels i and j at speed of order $N_i N_j$ where N_i is the number of points used at level i . This second algorithm performs more or less equally well as the first, and allows one to certify the results obtained.

In summary, this second algorithm works as follows. Depending on the physical parameters requested, an initial choice is made of the number n_{\max} of functions to be considered, and of the limits Δ_i at each level. A dynamical parameter called the running precision is initialized, which estimates the numerical accuracy obtained in computing the free energy using the points configuration used. The coupled equations are then iterated (possibly using extrapolations) in order to achieve a certain degree of convergence, measured by the condition that the total rate of flow of all points as the iterations proceed becomes smaller than the running precision.

At this point, a *cycle* is initiated. This entails a number of steps, with the objective of increasing the accuracy, *i.e.* of decreasing the running precision achieved. First, each function is examined in turn, and points are added in regions with larger curvature. Second, the limits Δ_i are extended (and points added) if the value of the function at the previous limit is not sufficiently close to its analytically-determined asymptotic value ϵ_i^∞ . Third, new functions are added (*i.e.* n_{\max} is increased) if the highest function is not sufficiently close to its asymptotic value throughout the k line. A new value of the running precision is then determined, based on the refinements just performed on the distribution of points. Finally, iterations are performed until the flow rate drops below this running precision.

For a specific set of physical parameters, a total allowed time is also given to the program. This second implementation then performs cycles one after the other, yielding increasingly accurate results, until the allowed time is exhausted. An estimate of the absolute accuracy of the whole procedure can thus be obtained by comparing the results from runs with different total allowed times.

IV. QUANTUM STATISTICS VERSUS TEMPERATURE FLUCTUATIONS

The $SU(2)$ degree of freedom in combination with the bosonic statistics in 1D leads to a macroscopic behavior: the polarization of the ground state. This phenomenon which occurs in every bosonic system with no explicit component-dependent forces, has been already proven in the literature [33]. We will give here an interpretation in

terms of the string structure of the Bethe solutions and provide a quantitative result for the persistence of this effect for non-zero temperature.

The polarization at zero temperature can be directly linked to the underlying string structure of the Bethe equation solutions. In eq. (3), the $\varepsilon(k)$ function depicts the charge degree of freedom and the $\varepsilon_n(k)$ functions the spin degrees of freedom. Moreover those latter functions express the dynamics of quasiparticle forming a colour 2 energetically disfavored state made of n particles. As the temperature of the system goes down, the contribution of these states in the equilibrium decreases.

We hereafter explain how at the limit $T = 0$ there only remains one spin-gapped state gathering all particles in the 1st component. In the YTY equations (3) where the $\varepsilon_n(k)$ are the dressed energies of an n -string, a phenomenological approach to $T = 0$ is possible. Taking the first line of (3) and approximating the values $\varepsilon_n(k) \approx 2n\Omega$, if one takes the limit $T \rightarrow 0$, $T \sum_{n=1}^{\infty} \ln [1 + \exp(-2\frac{n\Omega}{T})] \rightarrow 0$ as Ω is defined positive. The contribution of the colour 2 particles then disappears from the thermalized state and this reveals that the colour 1 component drives away all colour 2 particles, forming a fully polarized spin-gapped state. (In the Bethe equations, only the 2nd component part of the wave function is represented by quasiparticles). We show this expelling in figure 1 where we plot polarization curves (bottom set) as a function of μ . As the chemical potential increases, the interaction parameter, $\gamma (= \frac{c}{n_1+n_2})$ decreases monotonically and the polarization persists to higher temperatures. In [38], Fuchs et al. revealed that the effective mass of an isospin wave above the polarized ground state is very high in the strong coupling regime. Furthermore, it is surprising to see that when μ increases, the polarized ground state is more resistant to thermal fluctuation even though the isospin wave mass decreases.

In the context of spontaneous imbalance in binary mixtures [48–50], it has been shown that at zero temperature, a mixed gas is unstable and exhibits a spatial phase separation. But no quantitative predictions have been made for finite temperature in 1D. From figure 1, we see that the polarization remains at higher temperatures for high value of μ . By qualitative identification of the ferromagnetic behavior with the the spatial demixing, we can speculate that a phase separation would resist better to temperature in the low coupling regime than for $\gamma \gg 1$.

The figure 1 shows as well curves of polarization for fixed particle density, interaction strength and fixed Ω as a function of the reduced temperature, $\tau = \frac{T}{T_D}$ where $T_D = (n_1 + n_2)^2$ is the degeneracy temperature [46]. We compare these results with the polarization of an interaction-free 2CBG which is $\frac{n_1^0 - n_2^0}{n_1^0 + n_2^0} = \tanh(\Omega/k_B T)$. The non-negligible difference which appears between the curves of same Ω is the ferromagnetic effect which is a consequence of the bosons interaction.

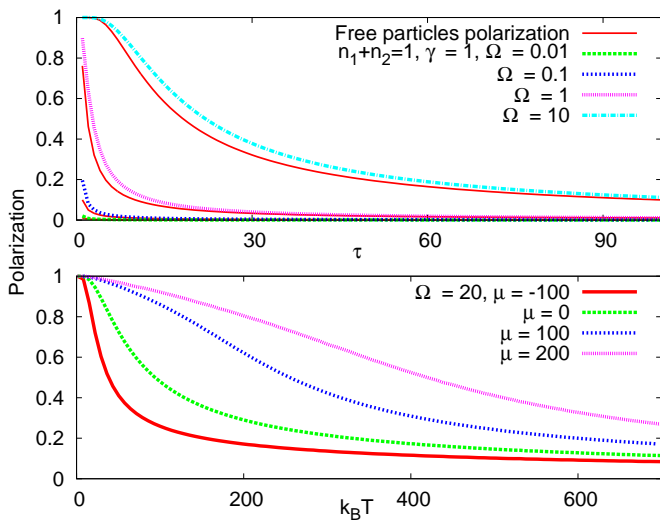


FIG. 1: The top graph shows polarization of the 2CBG , $(n_1 - n_2)/(n_1 + n_2)$, for fixed density of particles and interaction strength (γ) as a function of the reduced temperature (τ). The set of curves for several different Ω are compared to the curves of a free gas. The bottom plot shows the isobar polarization as a function of the temperature for four different chemical potentials: $\{-100, 0, 100, 200\}$. In this latter graph, the density γ and τ vary along the curves.

As T approaches zero, the gas polarizes and the remaining component behaves like a Lieb-Liniger gas of chemical potential $\mu_1 = \mu + \Omega$. The results are then comparable to the results of V. N. Popov [51] for the density of the Lieb-Liniger gas at $T = 0$ and $\gamma \ll 1$:

$$\rho(\mu) = \frac{\mu}{2c} + \frac{\sqrt{\mu}}{\sqrt{2\pi}} + c\left(\frac{1}{2\pi^2} - \frac{1}{24}\right) + \dots \quad (15)$$

As shown in Fig. 2, by lowering down the reduced temperature of the gas to $\tau \ll 1$, the total chemical potential corresponds to the zero temperature low coupling regime formula. Moreover, in this particular regime, the corresponding polarizations lines turn out to be almost constant along γ .

The specific heat capacity of the gas at fixed density of particles which is accessible via the entropy (9) provides a view on the thermal degrees of freedom of the system. Figure 3 shows that in a 2CBG at low temperature with strong Ω , the heat capacity is similar to that of a Lieb-Liniger Bose gas contributed by phonons. If the relative chemical potential is lower or of order of the temperature, the two component degree of freedom appears and creates peaks similarly to a paramagnetic spinor Bose gas [34]. The maximum in the specific heat moves in higher temperature as the relative chemical potential increases. The higher temperature results are shown in 4 where we can observe that the peaks are located when $\Omega \sim T$. At high temperature the gas becomes decoherent classical

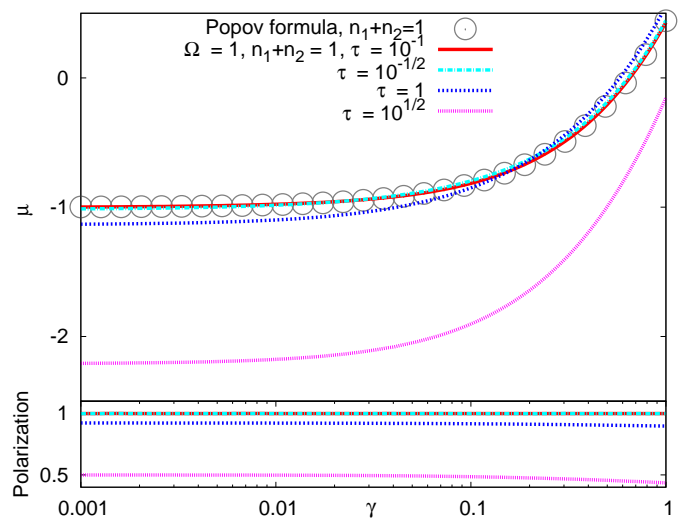


FIG. 2: For $\gamma \ll 1$, and $\tau \ll 1$, the 2CBG chemical potential follows the Popov's expression for the zero temperature Lieb-Liniger case.

(see VI) and the specific heat converges to $1/2$ which is the value of the simple 1D ideal gas.

Experiments trapping Helium-4 fluid into 1D nanopores [52] provide a possible realization of the 1D Bose gas and give access to measurement of the heat capacity of the unidimensional system. A similar realization with an isospin-1/2 might be possible and provide measurement of the 2CBG heat capacity.

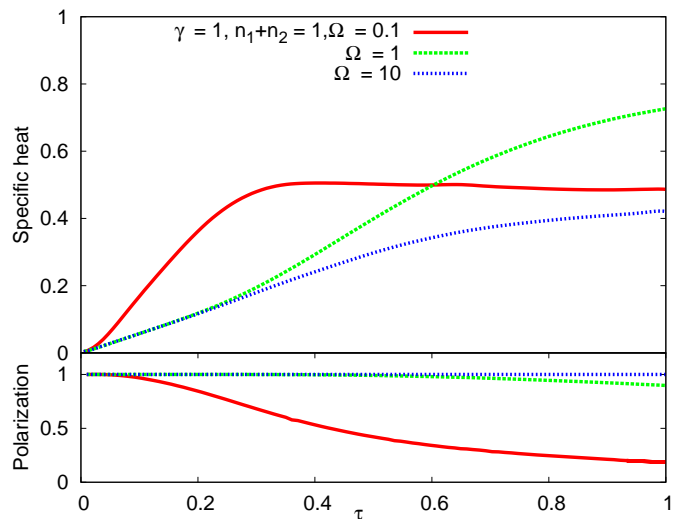


FIG. 3: The specific heat of the 2CBG for fixed density of particles and interaction strength as a function of the reduced temperature. The different chemical potentials of each curve have a value closed to γ . Similarly to a free 2CBG case, we see a peak in the specific heat whos the position depends on Ω .

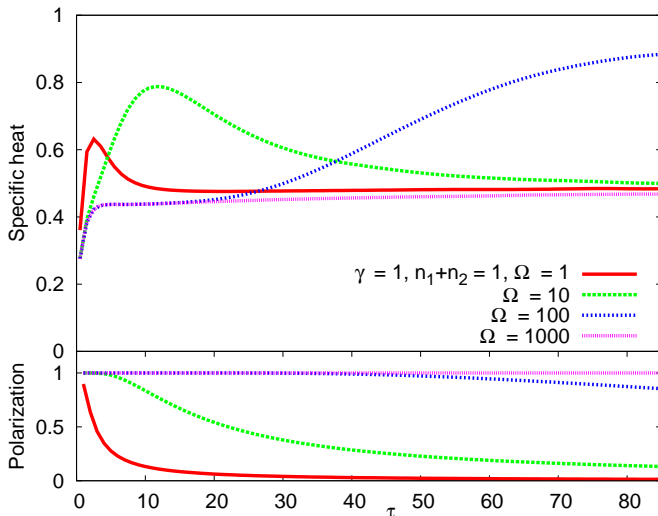


FIG. 4: The specific heat of the 2CBG for fixed density of particles and interaction strength as a function of the reduced temperature. The different chemical potentials have a value $\Omega \gg \gamma$. In the limit of high temperature, the gas becomes ideal and the specific heat takes the value $1/2$.

V. RESULTS IN THE INTERMEDIATE REGIME

In this section we will present the results that don't belong to a limit regime. Furthermore in those parameter ranges, we give numerical results for the polarization of the 2CBG and the local pair correlator where neither the thermal, the charge nor the phase fluctuations dominate. They compete in the 2CBG state and therefore no perturbative approach but only the thermodynamic Bethe ansatz can predict a solution. We will discuss and describe as much as possible the changes in behaviour that occur in these intermediate regimes.

The set of following graphs in figures 5 and 6 show the behaviour of the two component Bose gas as a function of γ and any fixed value of Ω, T . The values of Ω and T are chosen such that in each case the ratio $\frac{\Omega}{T}$ goes from less to more than 1. Following the qualitative description of [46, 47] for the single-component case, the regimes of the gas are identified by the two dimensionless parameters $\gamma = \frac{c}{n_1+n_2}$ and $\tau = \frac{T}{(n_1+n_2)^2}$, respectively the interaction strength and the reduced temperature. As results presented hereafter are made for fixed interaction parameter (c), the ratio $\frac{\tau}{\gamma^2} = \frac{T}{c^2}$ is then constant and the regime is identified by the position on the γ axis. At the lowest value of γ , $\gamma \lesssim \tau \ll 1$ and the gas quasicondenses in a Gross-Pitaevskii (GP) regime with thermal fluctuations. At the other end, where $\gamma > 1$, the regime is decoherent classical (DC) with $\tau \gg \max\{1, \gamma^2\}$. In the case of a quasicondensate, we see progressively the ferromagnetic effect

with a completely polarized gas whereas the polarization reaches the value of an ideal paramagnetic gas when the 2CBG becomes DC. From this simple view of the data, we can try to see how the temperature and the relative chemical potential modify these phenomena.

The first column of figure 5 shows the effects of the temperature on the polarization. In the region where $\gamma > 1$ the linear density of each component is almost classical and the asymptotic value of the curves are given by $\frac{e^{\beta\mu_1} - e^{\beta\mu_2}}{e^{\beta\mu_1} + e^{\beta\mu_2}}$ (see VI). Here the charge and coherent fluctuations are large and hence the statistics and the interaction of the gas don't play any role (the observables depend only on the temperature and chemical potentials). In contrast, for $\gamma \ll 1$ the gas quasicondenses and the charge fluctuations vanish. The ratio τ/γ^2 being large, the temperature fluctuations exceed the phase fluctuations and we see that T doesn't influence the polarization much.

The second column of data shows the variations of the polarization as a function of Ω . The spontaneous ferromagnetism in the presence of the quasicondensate happens in high interaction strength when the relative chemical potential increases. In the YYT equations (3), the effect of Ω on the strings appears through the asymptotic value of the contribution of the n -strings: $T \sum_{n=1}^{\infty} \ln [1 + \exp(-2\frac{n\Omega}{T})]$. When Ω increases, the colour 2 spin-gapped state effect are suppressed and the polarization resists higher charge fluctuation (higher γ).

Figure 6 shows the local density-density correlation function as a function of γ for different values of the relative chemical potential and temperature. On the top graph the ratio τ/γ^2 is fixed; for $\gamma \ll 1$, the 2CBG is thus in a quasicondensate with important thermal fluctuations. In this regime the gas is ferromagnetic and Ω has no effect on the correlation. On the other hand, for large values of γ , the gas is DC and the asymptotic value of $g^{(2)}$ follows from Wick's theorem and the Boltzman distribution, $g_0^{(2)} = 1 + \frac{\sum_i e^{2\beta\mu_i}}{(\sum_i e^{\beta\mu_i})^2}$. The first order corrections will be calculated later (VI). In the bottom figure, the curves for different temperatures show the nonmonotonic behaviour discussed in [40]. Close to the quasicondensate regime, the pair correlation increases with temperature: in the DC regime temperature has a destructive role on the correlation.

VI. DECOHERENT REGIMES

In the limit of the weakly interacting Bose gas, ($\gamma \ll \min\{\tau^2, \sqrt{\tau}\}$) or in the high temperature regime ($\tau \ll \max\{1, \gamma^2\}$), the phase and density fluctuations are large. Therefore one can notice that in the YYT equations 3, the limit of either high temperature, $T^{-1} = \delta \ll 1$ with finite c , or low coupling $c = \delta \ll 1$ with $T \neq 0$, one recovers the thermodynamics of two ideal Bose gases

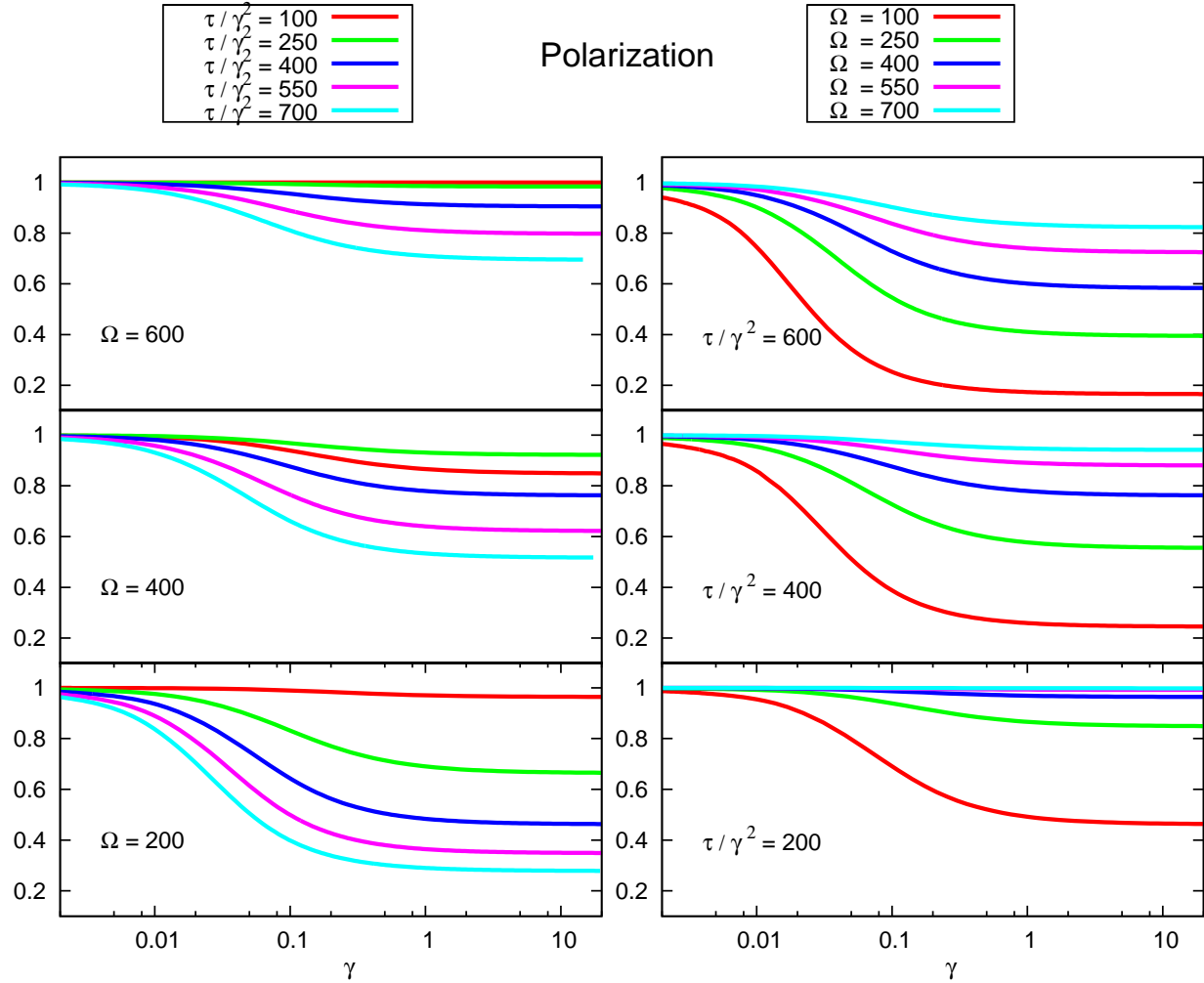


FIG. 5: Polarization of the 2 component Bose gas as a function of the interaction strength γ for fixed values of $\Omega (= \frac{\mu_1 - \mu_2}{2})$ and for fixed ratios τ/γ^2 .

up to $\mathcal{O}(\delta^2)$. In this limit the convolutions of a function g with the kernels described in equations (3) become:

$$\begin{aligned} a_n * g(k) &= \int_{-\infty}^{\infty} d\bar{k}' \frac{1}{\pi} \underbrace{\frac{nc/(2\sqrt{T})}{(nc/(2\sqrt{T}))^2 + (\bar{k} - \bar{k}')^2}}_{\lim_{\delta \rightarrow 0} \delta(\bar{k} - \bar{k}')} \cdot g(\bar{k}'\sqrt{T}) \\ &= g(\bar{k}\sqrt{T}) \end{aligned} \quad (16)$$

$$\begin{aligned} f * g(k) &= \int_{-\infty}^{\infty} d\bar{k}' \frac{\sqrt{T}}{\cosh(\frac{\pi}{c}\sqrt{T}(\bar{k} - \bar{k}'))} \cdot g(\bar{k}'\sqrt{T}) \\ &= cg(\bar{k}\sqrt{T}) \end{aligned} \quad (17)$$

Furthermore the Gibbs free energy resulting from this

simplified system is:

$$\begin{aligned} \frac{G}{L} &= -\frac{T}{2\pi} \int_{-\infty}^{\infty} \ln \left[1 + e^{-\varepsilon(k)/T} \right] dk \\ &= \frac{T}{2\pi} \int_{-\infty}^{\infty} \ln \left[\left(1 - e^{(\mu_1 - k^2)/T} \right) \right] dk \\ &\quad + \frac{T}{2\pi} \int_{-\infty}^{\infty} \ln \left[\left(1 - e^{(\mu_2 - k^2)/T} \right) \right] dk \end{aligned} \quad (18)$$

which is the sum of the Gibbs energy of two ideal Bose gases.

First order corrections can then be effectively described using perturbation theory and the reduced temperature, $\tau = \frac{T}{(n_1 + n_2)^2}$, allows one to distinguish between the decoherent quantum regime (DQ) for $\sqrt{\gamma} \ll \tau \ll 1$ and the decoherent classical (DC) regime with $\tau \gg \max\{1, \gamma^2\}$ [46, 47, 53].

We use Feynman diagrams to express the perturbed

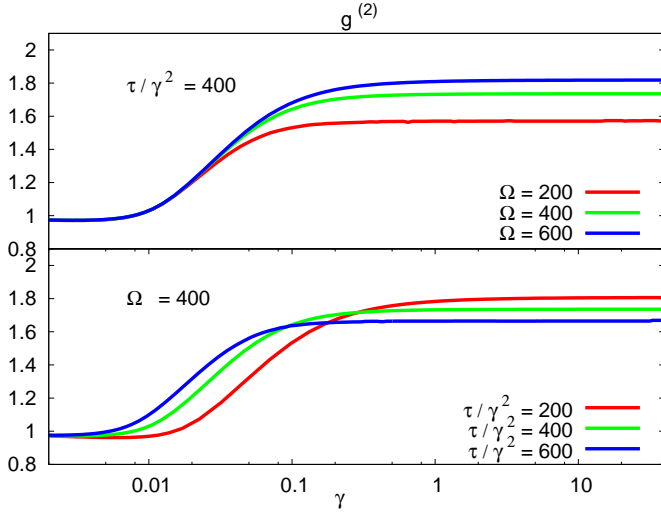


FIG. 6: The local pair correlation $g^{(2)}$ of the 2 component Bose gas as a function of the interaction strength γ and for fixed values of Ω and for fixed ratio τ/γ^2 .

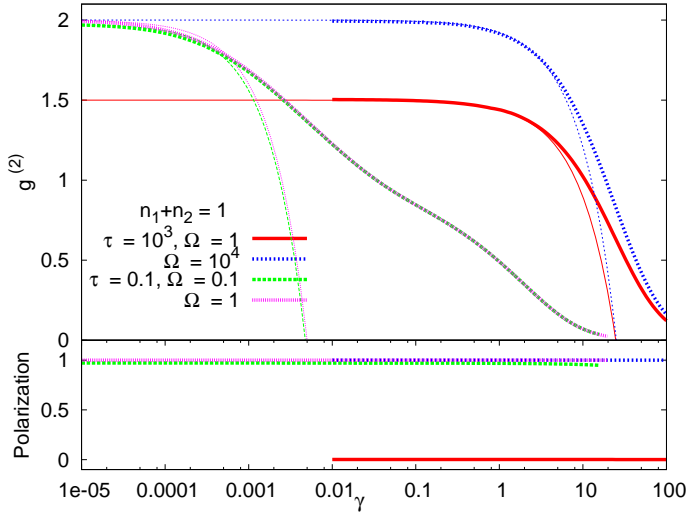


FIG. 7: Comparison between the numerical (thick lines) and the analytical results (thin lines) in the decoherent quantum regime, $\sqrt{\gamma} \ll \tau \ll 1$ (22) and in the decoherent classical regime, $\tau \gg \max\{1, \gamma^2\}$ (23). The reduced temperature is fixed either to $\tau = 0.1$ with $\Omega = 0.1, 1$ for a decoherent quantum gas or to $\tau = 1000$ with $\Omega = 1, 10^4$ for a classical decoherent gas. At high value of the interaction strength when $\gamma \gg 1$, the 2CBG enter a fermionization regime.

Gibbs free energy. An explicit expression is then calculated for the local pair correlation function, $g^{(2)}$ in the two decoherent regimes (DQ & DC) to first order.

The partition function of the 2 component 1D Bose gas in the Feynman path integral formalism is

$$Z = \int \mathcal{D}(\bar{\Psi}, \Psi) e^{-S[\bar{\Psi}, \Psi]}$$

$$S[\bar{\Psi}, \Psi] = \int_0^\beta d\tau \int dr \sum_a \bar{\Psi}_a \partial_\tau \Psi_a - \mathcal{H}(\bar{\Psi}, \Psi) \quad (19)$$

where $\Psi(r, \tau)$ is a space and imaginary time-dependent spin-1/2 field and \mathcal{H} is the Hamiltonian density from (1). At first order, the correction to the Gibbs free energy following from Wick's theorem is $G^{(1)} = 2c [n^{02} - n_0^0 n_1^0] + \mathcal{O}(c^2)$ with the free linear density of the a -th component: $n_a^0 = \frac{T}{L} \sum_{k,n} \frac{1}{i\hbar\omega_n - \hbar^2 k^2 / 2m + \mu_a}$ and the total free linear density: $n^0 = \sum_a n_a^0$. For the second order in c , the diagrammatic representation gives five contributions shown in figure 8 that give the free energy density corrections:

$$G^{(2)} = -\frac{c^2}{2} \left[\overbrace{8 n^0 \sum_b n_b^0 \partial_{\mu_b} n_b^0}^{b)} + 4 n^{02} \sum_b \partial_{\mu_b} n_b^0 \overbrace{\quad}^{a)} + 4 \underbrace{\sum_a (n_a^0)^2 \partial_{\mu_a} n_a^0}_d + 2 \sum_{a=0,1} \left(\underbrace{P_{a,a}}_c + \underbrace{P_{a,a} + P_{a,|a-1|}}_e \right) \right] + \mathcal{O}(c^3) \quad (20)$$

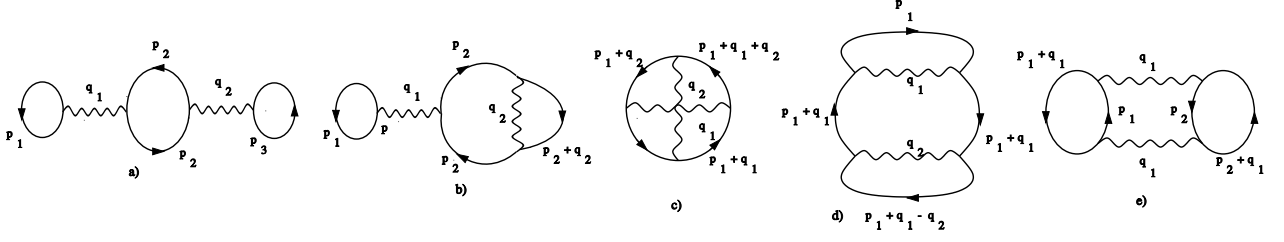


FIG. 8: Connected Feynman diagrams in second order perturbation of interaction. Labels are related to terms of eq. (20)

where the first three terms correspond to the diagrams b), a) and d) and where c) and e) provide the last terms

containing the double polarization bubbles which are defined as

$$P_{a,b} = \sum_m \int_{-\infty}^{\infty} dk \left(\sum_n \int_{-\infty}^{\infty} dl G_{a,m+n}(k+l) G_{a,n}(l) \sum_{n'} \int_{-\infty}^{\infty} dl' G_{b,m+n'}(k+l') G_{b,n'}(l') \right) \quad (21)$$

with the Green function $G_{a,n}(l) = \frac{1}{i\hbar\omega_n - \hbar^2 l^2 / 2m + \mu_a}$. The local pair correlation results from equation (10) and an analytic expression as a function of c, T, μ_i is given in the two decoherent regimes. In the DQ regime, $\sqrt{\gamma} \ll \tau \ll 1$ and $\mu_1, \mu_2 \ll T$, by taking the leading order in the Bose occupation number, the free linear density

is $n_a^0 = \frac{T}{2\sqrt{-\mu_a}}$ and the double polarization bubble is $P_{a,b} = \frac{n_a^0 + n_b^0 - (n_a^{02} + n_b^{02}) / (n_a^0 + n_b^0)}{\tau_a \tau_b}$. For a compact notation we define the a th component reduced temperature by $\tau_a = \frac{T}{n_a^{02}}$. We find so the local pair correlation to be

$$g^{(2)} = \frac{n^{02} + \sum_i n_i^{02}}{n^{02}} + 4\gamma \left[\frac{2}{\tau_1 \tau_2} - \frac{1}{n^{02}} \left(\frac{n_1^0}{\tau_1^2} + \frac{n_2^0}{\tau_2^2} \right) \right] - 4\gamma \frac{n^{02} - \sum_i n_i^{02}}{n^{02}} \left[4 \left(\frac{1}{\tau_1^2} + \frac{1}{\tau_2^2} \right) + \frac{1}{\tau_1 \tau_2} \right] + \mathcal{O}(\gamma^2) \quad (22)$$

In the DC regime, $\tau \gg \max\{1, \gamma^2\}$ and $\mu_1, \mu_2 \gg T$, the bosonic occupation number becomes the Boltzmann distribution and $n_a^0 = \sqrt{\frac{\pi}{\beta} \frac{e^{\beta\mu_a}}{2}}$, $P_{a,b} = n_a^0 n_b^0 \sqrt{\frac{\pi\beta}{8}}$. The

pair correlator becomes

$$g^{(2)} = \frac{n^{02} + \sum_i n_i^{02}}{n^{02}} - \sqrt{\frac{\pi}{2}} \gamma \left(\frac{1}{\sqrt{\tau_1}} + \frac{1}{\sqrt{\tau_2}} \right) \left[\frac{n^{02} + \sum_i n_i^{02}}{n^{02}} \right] + \frac{4\gamma}{\sqrt{\tau_1 \tau_2}} \left[1 - 2 \frac{n^{02} - \sum_i n_i^{02}}{n^{02}} \right] + \mathcal{O}(\gamma^2) \quad (23)$$

In order to illustrate this result, we compare the value of $g^{(2)}$ computed to the first order in γ (eq.22 and 23) with the numerical results using (10) in figure 7. The curves calculated at fixed particle density and reduced temperature show that the numerical results follow nicely

the analytical expansion until either the thermal fluctuations become too strong for the DQ gas ($\gamma \sim 10^{-3}$) or the charge fluctuations become important in the DC regime when $\gamma \sim 10$. As the interaction strength increases, we progressively switch to a high temperature

Tonks-Girardeau like fermionization regime for the DC curves and to a ferromagnetic fermionization for the DQ case. It would be interesting as well to compare the results for a DQ gas in very low Ω such that the polarization is low and $g^{(2)}$ reaches the value $3/2$ but this implies a calculation for a very high number of functions, n_{max} with a large number of points. We couldn't afford then the number of iterations necessary to have a converged solution.

VII. TONKS-GIRARDEAU REGIME

In the extreme case of impenetrable particles ($\gamma \rightarrow \infty$), M. Girardeau [21] showed the correspondence between impenetrable Bose and Fermi wave functions. While the statistics of the bosons wave function remains symmetric, there is no more overlap between the neighbor particles. In the case of 2CBG, the charge part of the wave function behave like a one-component free fermion gas and non-interacting distinguishable spin- $1/2$ since any spin-spin exchange vanishes [34, 39, 44]. In both 1CBG and 2CBG, the local density-density correlation function then naturally vanishes since there is no double space occupancy.

In the strong coupling regime ($\gamma \gg \max(1, \sqrt{\tau})$) with quantum degeneracy ($\tau \ll 1$), the finite-temperature corrections are markedly different in a Lieb-Liniger gas [46] and the spinor Bose gas [34] with a different exponent. In figure 9, bottom part, we represent this analytical result at zero temperature (thin line) next to numerical results with decreasing temperature for fixed density of particles. We observe that for $\gamma \gg 10$, the value of $g^{(2)}$ decreases with τ and converges to this $T = 0$ analytical result where the 2CBG is ferromagnetic and doesn't depend on Ω . For a high-temperature fermionization ($\gamma^2 \gg \tau \gg 1$), Kheruntsyan et al. [46] give the first order correction in τ/γ^2 for $g^{(2)}$ for a Lieb-Liniger gas. However the approach of free fermions with a $1/\gamma$ perturbation is not applicable in the two component case, therefore the correction to the fermionization regime are unknown. In figure 9, top part, we show next to the 1 component asymptotic curve, the decay of $g^{(2)}$ for a fixed reduced temperature and various relative chemical potential. As Ω reaches 100, the 2CBG polarization is saturated and the correlator decays like a Lieb-Liniger gas.

VIII. CONCLUSION

In conclusion, we have studied the equilibrium thermodynamic properties of exactly solvable interacting one-dimensional two-component Bose gas systems as a function of their external canonical or grand canonical parameters (either temperature, interaction strength and total

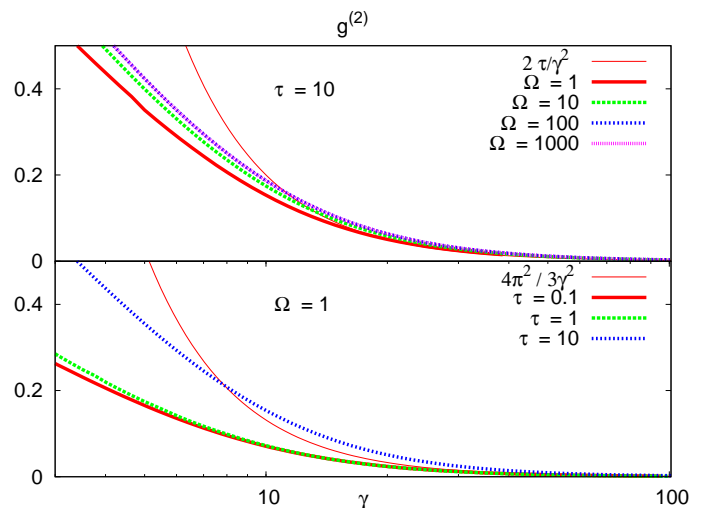


FIG. 9: In the Tonks-Girardeau regime, the pair-pair correlation decay to zero when the correlation strength becomes large ($\gamma \gg \max(1, \sqrt{\tau})$). The top graph shows the high-temperature fermionization and its dependence in Ω . The 1CBG asymptotic behavior in τ/γ^2 is also shown in comparison with the fully polarized 2CBG ($\Omega \gg T$). In the bottom graph we show curves with different reduced temperatures that we compare with the analytical expression at zero temperature [34]. The 2CBG is here ferromagnetic and the value of $g^{(2)}$ doesn't depend on the relative chemical potential.

and relative chemical potential or temperature, interaction strength, density of particle and relative chemical potential). Our method was based on the solution of thermodynamic Bethe ansatz equations and yields quantitative predictions which should be experimentally accessible using cold atomic systems. We particularly would like to clarify that solving the non linear integrable equations is possible with a very good control of numerical precision.

Note: as our manuscript was being completed, a different but equivalent set of equations was proposed in [54]. While this set of equations is at first sight more economical, we find and demonstrate here that the solution of the infinite set of TBA equations is feasible and practical, robust and reliable. The TBA dressed energies in 3 are relatively smooth functions of a real variable, while the functions of [54] are of a complex variable. The computational effort required by the two methods are thus probably comparable. On the other hand, the fact that results from this alternate method coincide with our results here (and our earlier summary [40]) interestingly confirms that the string hypothesis can be trusted when computing equilibrium thermodynamic results, as expected from general arguments based on the structure of the Bethe equations [55].

Appendix A: Thermodynamics from Bethe Ansatz

We model the system of 2 component bosons with SU(2) bosonic fields evolving in a 1 dimensional continuum space of length L with a delta-function interaction. The Hamiltonian is then:

$$H = \int_0^L dx \sum_{a \in \{-1,1\}} \partial_x \Psi_a^\dagger(x) \partial_x \Psi_a(x) + c \sum_{b,a \in \{-1,1\}} \Psi_a^\dagger(x) \Psi_b^\dagger(x) \Psi_b(x) \Psi_a(x) \quad (\text{A1})$$

With $c = \frac{g_{1D} \cdot m}{\hbar^2}$, g_{1D} the 1D coupling constant and m the mass of the bosons.

Integrating the string structure, $\lambda_{\alpha,j}^n = \Lambda_\alpha^n + \frac{ic}{2}(n + 1 - 2j)$, $j = 1, \dots, n$, in the scattering equations in (2) and defining $e_n(\lambda) = \frac{\lambda - icn/2}{\lambda + icn/2}$, the scattering equations become:

$$e^{ik_j L} = - \prod_{l=1}^N \frac{k_j - k_l + ic}{k_j - k_l - ic} \prod_{n=1}^{\infty} \prod_{\alpha=1}^{N_n} \frac{k_j - \Lambda_\alpha^n - \frac{inc}{2}}{k_j - \Lambda_\alpha^n + \frac{inc}{2}}$$

$$\prod_{p=1}^N \frac{k_p - \Lambda_\alpha^n + \frac{inc}{2}}{k_p - \Lambda_\alpha^n - \frac{inc}{2}} = (-1)^n \prod_{m,\beta} \begin{cases} e_2^2(\Lambda) e_4^2(\Lambda) e_{n-m+4}^2(\Lambda) \dots e_{2n-2}^2(\Lambda) e_{2n}(\Lambda), & m = n \\ e_{n-m}(\Lambda) e_{n-m+2}^2(\Lambda) e_{n-m+4}^2(\Lambda) \dots e_{n+m-2}^2(\Lambda) e_{n+m}(\Lambda), & m \neq n \end{cases} \quad (\text{A2})$$

with the notation: $\Lambda = \Lambda_\alpha^n - \Lambda_\beta^m$.

In logarithm form, with $\frac{1}{i} \ln(e_n(\Lambda)) = \phi_n(\Lambda) = -\pi + 2 \operatorname{atan}(\frac{\Lambda}{cn/2})$, we have:

$$k_j = 2\pi \frac{I_j}{L} - \frac{1}{L} \sum_{l=1}^N \phi_2(k_j - k_l) + \frac{1}{L} \sum_{n=1}^{\infty} \sum_{\alpha=1}^{N_n} \phi_n(k_j - \Lambda_\alpha^n)$$

$$\frac{1}{L} \sum_{p=1}^N \phi_n(k_p - \Lambda_\alpha^n) = \frac{1}{L} 2\pi J_\alpha^n$$

$$+ \frac{1}{L} \sum_{m=1}^{\infty} \sum_{\beta=1}^{N_m} \begin{cases} 2\phi_2(\Lambda_\alpha^n - \Lambda_\beta^m) + 2\phi_4(\Lambda_\alpha^n - \Lambda_\beta^m) \dots \phi_{2n}(\Lambda_\alpha^n - \Lambda_\beta^m), & m = n \\ \phi_{|n-m|}(\Lambda_\alpha^n - \Lambda_\beta^m) + 2\phi_{|n-m|+2}(\Lambda_\alpha^n - \Lambda_\beta^m) \dots \phi_{n+m}(\Lambda_\alpha^n - \Lambda_\beta^m), & m \neq n \end{cases} \quad (\text{A3})$$

$\{I_j\}$ is a set of N numbers in $\mathbb{Z} + \frac{1}{2}$ and $\{J_\alpha^n\}$ are M_n sets of n numbers in \mathbb{Z} ($\mathbb{Z} + \frac{1}{2}$) if M_n is even (odd). These Bethe equations map the sets $\{I_j\}, \{J_\alpha^n\}$ to the set of rapidities and isospin-rapidities, $\{k_j\}$ and $\{\Lambda_\alpha^n\}$.

1. Thermodynamic limit

In the limit $N, L \rightarrow \infty$ with the ratio $\frac{N}{L}$ kept constant, the sets of rapidities ($\{k_j\}$ and $\{\Lambda_\alpha^n\}$) and quantum numbers ($\{I_j\}$ and $\{J_\alpha^n\}$) are replaced by continuous functions of particle root densities in real parameter space:

$$\rho(x) = \frac{1}{L} \sum_j \delta(x - \frac{I_j}{L}), \rho(k') = \frac{1}{L} \sum_j \delta(k - k_j(\frac{I_j}{L}))$$

$$\sigma^n(y) = \frac{1}{L} \sum_j \delta(y - \frac{J_\alpha^n}{L}),$$

$$\sigma^n(\Lambda') = \frac{1}{L} \sum_j \delta(\Lambda - \Lambda_\alpha^n(\frac{J_\alpha^n}{L})), \forall n \quad . \quad (\text{A4})$$

Hole densities, ρ_h, σ_h^n are similarly defined from the complementary sets $\{\tilde{I}_i\}, \{\tilde{J}_\alpha^n\}$, and the total root densities are $\rho_t(k) = \rho_h(k) + \rho_h(k)$ and $\sigma_t^n(\Lambda) = \sigma_h^n(\Lambda) + \sigma_h^n(\Lambda)$. The thermodynamic limit allows one to replace the dis-

crete sum by an integral over a continuum.

$$\rho_t(x) = \frac{1}{L} \sum_{I \in \{I_i\}, \{I_i\}} \delta(x - \frac{I}{L}) \xrightarrow{\text{Th.L.}} \int_{-\infty}^{\infty} dx' \delta(x - x') = 1$$

$$\sigma_t^n(y) \xrightarrow{\text{Th.L.}} 1 \quad (\text{A5})$$

and the indexations of the rapidities by the quantum numbers, $(k_j(\frac{I_j}{L}), \Lambda_\alpha^n(\frac{J_\alpha^n}{L}))$ become continuous functions : $k(x)$ and $\Lambda^n(y)$. An important point of the thermody-

amic limit is the assumption that all the density functions are in \mathcal{C}^∞ . However some sets of $\{I_j\}$, $\{J_\alpha^n\}$ that are solutions of (A2), could provide no differentiable functions. For instance if all the rapidities are grouped in a block Fermi-sea like. But the role of these solutions play a negligible role in the thermodynamic limit due to the fact that their weight in the set of all solutions goes to zero. Physically, they represent the solutions with low entropy. Finally, under the thermodynamic limit (A3) becomes:

$$k(x) = 2\pi x - \int_{-\infty}^{\infty} \phi_2(k - k') \rho(k') dk' + \sum_{m=1}^{\infty} \int_{-\infty}^{\infty} \phi_m(k - \Lambda) \sigma^m(\Lambda) d\Lambda$$

$$\int_{-\infty}^{\infty} \phi_n(k - \Lambda) \rho(k) dk = 2\pi y$$

$$+ \sum_{m=1}^{\infty} \int_{-\infty}^{\infty} \sigma^m(\Lambda') d\Lambda' \begin{cases} 2\phi_2(\Lambda - \Lambda') + \dots + \phi_{2n}(\Lambda - \Lambda'), & m = n \\ \phi_{|n-m|}(\Lambda - \Lambda') + \dots + \phi_{n+m}(\Lambda - \Lambda'), & m \neq n \end{cases} \quad (\text{A6})$$

2. YYT equations

Following the method of C. N. Yang and C. P. Yang [45], the equilibrium state is determined by minimization

of the Gibbs free energy in the grand canonical ensemble. With G the Gibbs free energy, E the internal energy, S the entropy, we have:

$$G = E - TS - \mu_1 N_1 - \mu_2 N_2$$

$$\frac{E}{L} = \int_{-\infty}^{\infty} dk \rho(k) k^2$$

$$\frac{S}{L} = \int_{-\infty}^{\infty} dk [(\rho + \rho_h) \ln(\rho + \rho_h) - \rho \ln(\rho) - \rho_h \ln(\rho_h)] + \sum_{n=0}^{\infty} \int_{-\infty}^{\infty} dk [(\sigma^n + \sigma_h^n) \ln(\sigma^n + \sigma_h^n) - \sigma^n \ln(\sigma^n) - \sigma_h^n \ln(\sigma_h^n)]$$

$$\mu_1 n_1 + \mu_2 n_2 = \int_{-\infty}^{\infty} dk \Omega \left(\rho - 2 \sum_n n \sigma^n \right) + \mu \rho \quad (\text{A7})$$

with L the length of our system, $n_i = \frac{N_i}{L}$ the density of i th component particles and $\mu = \frac{\mu_1 + \mu_2}{2}$, $\Omega = \frac{\mu_1 - \mu_2}{2}$. The

condition of equilibrium is then:

$$\delta \rho \frac{\partial G}{\partial \rho} + \delta \rho_h \frac{\partial G}{\partial \rho_h} + \sum_n \delta \sigma^n \frac{\partial G}{\partial \sigma^n} + \delta \sigma_h^n \frac{\partial G}{\partial \sigma_h^n} = 0 \Big|_{\rho, \sigma^n \text{ solution of BE}} \quad (\text{A8})$$

from which one derives:

$$\begin{aligned}\varepsilon(k) &= k^2 - \mu - \Omega - T \cdot a_2 * \ln(1 + e^{-\varepsilon/T}) - \sum_n T \cdot a_n * \ln(1 + e^{-\varepsilon_n/T}) \\ \varepsilon_n(k) &= 2n\Omega + T \cdot a_n * \ln(1 + e^{-\varepsilon/T}) + T \cdot \sum_m T_{mn} * \ln(1 + e^{-\varepsilon_m/T}), \quad n = 1, 2, \dots\end{aligned}\quad (\text{A9})$$

with

$$T_{nm}(\Lambda) = \begin{cases} 2a_2(\Lambda) + 2a_4(\Lambda) \dots a_{2n}(\Lambda), & m = n \\ a_{|n-m|}(\Lambda) + 2a_{|n-m|+2}(\Lambda) \dots a_{n+m}(\Lambda), & m \neq n \end{cases} \quad (\text{A10})$$

$$\varepsilon(k) = T \ln\left(\frac{\rho_h(k)}{\rho(k)}\right) \quad (\text{A11})$$

$$\varepsilon_n(k) = T \ln\left(\frac{\sigma_h^n(k)}{\sigma^n(k)}\right) \quad (\text{A12})$$

The term T_{mn} which implies a coupling between every $\varepsilon_m(k)$ would severely slow down any numerical solving. But following the development of M. Takahashi [43, 44],

the system is partially decoupled and this term disappears:

$$\varepsilon(k) = k^2 - \mu - \Omega - T \cdot \left(a_2 * \ln \left[1 + \exp\left(-\frac{\varepsilon}{T}\right) \right] \right) (k) - T \sum_{n=1}^{\infty} \left(a_n * \ln \left[1 + \exp\left(-\frac{\varepsilon_n}{T}\right) \right] \right) (k) \quad (\text{A13})$$

$$\varepsilon_n(k) = \frac{T}{2c} \left\{ f * \left(\ln \left[1 + \exp\left(\frac{\varepsilon_{n+1}}{T}\right) \right] + \ln \left[1 + \exp\left(\frac{\varepsilon_{n-1}}{T}\right) \right] \right) \right\} (k), \quad (n \neq 1) \quad (\text{A14})$$

$$\varepsilon_1(k) = \frac{T}{2c} \left\{ f * \left(\ln \left[1 + \exp\left(\frac{\varepsilon_2}{T}\right) \right] + \ln \left[1 + \exp\left(-\frac{\varepsilon}{T}\right) \right] \right) \right\} (k) \quad (\text{A15})$$

with the convolution notation: $(f * g)(k) = \int f(k - k')g(k')dk'$, $a_n(k) = \frac{1}{\pi} \frac{nc/2}{(nc/2)^2 + k^2}$, $f(k) = 1/\cosh(\frac{\pi}{c}k)$.

We can easily calculate the two asymptotic limit similarly to the results for the isotropic spin chain of

M.Takahashi [44]:

$$\lim_{n \rightarrow \infty} \frac{\varepsilon_n(k)}{n} = 2\Omega \quad (\text{A16})$$

$$\lim_{k \rightarrow \infty} \varepsilon_n(k) (\equiv \varepsilon_n^\infty) = 2\Omega n + T \cdot \ln \left[\left(\frac{1 - \exp(-\frac{2\Omega}{T}(n+1))}{1 - \exp(-\frac{2\Omega}{T})} \right)^2 - \exp(-\frac{2\Omega}{T}n) \right] \quad (\text{A17})$$

Appendix B: Dressed energy derivatives

The derivatives of $\varepsilon(k)$ and $\varepsilon_n(k)$ are useful for calculation of free energy derivatives. Differentiating (3) and (A17) by $\nu = \mu, \Omega$, we get:

$$\begin{aligned}
\frac{\partial \varepsilon}{\partial \nu}(k) &= -1 + \left(a_2 * \frac{\partial \varepsilon / \partial \nu}{1 + \exp(\frac{\varepsilon}{T})} \right) (k) + \sum_{n=1}^{\infty} \left(a_n * \frac{\partial \varepsilon_n / \partial \nu}{1 + \exp(\frac{\varepsilon_n}{T})} \right) (k) \\
\frac{\partial \varepsilon_n}{\partial \nu}(k) &= \frac{1}{2c} \left[f * \left(\frac{\partial \varepsilon_{n+1} / \partial \mu}{1 + \exp(-\frac{\varepsilon_{n+1}}{T})} + \frac{\partial \varepsilon_{n-1} / \partial \nu}{1 + \exp(-\frac{\varepsilon_{n-1}}{T})} \right) \right] (k), (n \neq 1) \\
\frac{\partial \varepsilon_1}{\partial \nu}(k) &= \frac{1}{2c} \left[f * \left(\frac{\partial \varepsilon_2 / \partial \nu}{1 + \exp(-\frac{\varepsilon_2}{T})} - \frac{\partial \varepsilon / \partial \mu}{1 + \exp(\frac{\varepsilon}{T})} \right) \right] (k) \\
\lim_{n \rightarrow \infty} \frac{\partial \varepsilon_n / \partial \Omega(k)}{n} &= 2 \\
\frac{\partial \varepsilon_n^\infty}{\partial \Omega} &= \frac{2(1 - \exp(-\frac{2\Omega}{T}(n+1)))}{(1 - \exp(-\frac{2\Omega}{T})) (1 - \exp(-\frac{2\Omega}{T}n)) (1 - \exp(-\frac{2\Omega}{T}(n+2)))} \\
&\quad \cdot \left(n - n \cdot \exp(-\frac{2\Omega}{T}(n+2)) + (n+2) \cdot \exp(-\frac{2\Omega}{T}(n+1)) - (n+2) \cdot \exp(-\frac{2\Omega}{T}) \right)
\end{aligned} \tag{B1}$$

with the derivatives of the asymptotes for $\nu = \mu$ being identically zero. Differentiating by T gives:

$$\begin{aligned}
\frac{\partial \varepsilon}{\partial T}(k) &= \frac{\varepsilon(k) - k^2 + \mu + \Omega}{T} + \left(a_2 * \frac{\partial \varepsilon / \partial T - \varepsilon / T}{1 + \exp(\frac{\varepsilon}{T})} \right) (k) + \sum_{n=1}^{\infty} \left(a_n * \frac{\partial \varepsilon_n / \partial T - \varepsilon_n / T}{1 + \exp(\frac{\varepsilon_n}{T})} \right) (k) \\
\frac{\partial \varepsilon_n}{\partial T}(k) &= \frac{\varepsilon_n(k)}{T} + \frac{1}{2c} \left[f * \left(\frac{\partial \varepsilon_{n+1} / \partial T - \varepsilon_{n+1} / T}{1 + \exp(-\frac{\varepsilon_{n+1}}{T})} + \frac{\partial \varepsilon_{n-1} / \partial T - \varepsilon_{n-1} / T}{1 + \exp(-\frac{\varepsilon_{n-1}}{T})} \right) \right] (k), \quad (n \neq 1) \\
\frac{\partial \varepsilon_1}{\partial T}(k) &= \frac{\varepsilon_1(k)}{T} + \frac{1}{2c} \left[f * \left(\frac{\partial \varepsilon_2 / \partial T - \varepsilon_2 / T}{1 + \exp(-\frac{\varepsilon_2}{T})} - \frac{\partial \varepsilon / \partial T - \varepsilon / T}{1 + \exp(\frac{\varepsilon}{T})} \right) \right] (k) \\
\lim_{n \rightarrow \infty} \frac{\partial \varepsilon_n / \partial T(k)}{n} &= 0 \\
\frac{\partial \varepsilon_n^\infty}{\partial T} &= \ln \left[\left(\frac{1 - \exp(-\frac{2\Omega}{T}(n+1))}{1 - \exp(-\frac{2\Omega}{T})} \right)^2 - e^{-\frac{2\Omega}{T}n} \right] + \\
&\quad \frac{2\Omega}{T} \frac{2 \exp(-\frac{2\Omega}{T}) \frac{(1 - \exp(-\frac{2\Omega}{T}(n+1)))^2}{(1 - \exp(-\frac{2\Omega}{T}))^3} - n \exp(-\frac{2\Omega}{T}n) - 2(n+1) \exp(-\frac{2\Omega}{T}(n+1)) \frac{1 - \exp(-\frac{2\Omega}{T}(n+1))}{(1 - \exp(-\frac{2\Omega}{T}))^2}}{\left(\frac{1 - \exp(-\frac{2\Omega}{T}(n+1))}{1 - \exp(-\frac{2\Omega}{T})} \right)^2 - e^{-\frac{2\Omega}{T}n}}
\end{aligned} \tag{B2}$$

And by c :

$$\begin{aligned}
\frac{\partial \varepsilon(k)}{\partial c} &= -T \cdot \left(\frac{\partial a_2}{\partial c} * \ln \left[1 + \exp\left(-\frac{\varepsilon}{T}\right) \right] \right) (k) - T \sum_{n=1}^{\infty} \left(\frac{\partial a_n}{\partial c} * \ln \left[1 + \exp\left(-\frac{\varepsilon_n}{T}\right) \right] \right) (k) \\
&+ \left(a_2 * \frac{\partial \varepsilon / \partial c}{1 + \exp(\frac{\varepsilon}{T})} \right) (k) + \sum_{n=1}^{\infty} \left(a_n * \frac{\partial \varepsilon_n / \partial c}{1 + \exp(\frac{\varepsilon_n}{T})} \right) (k) \\
\frac{\partial \varepsilon_n(k)}{\partial c} &= \frac{T}{2c} \left[\left(\frac{\partial f}{\partial c} - \frac{f}{c} \right) * \left(\ln \left[1 + \exp\left(\frac{\varepsilon_{n+1}}{T}\right) \right] + \ln \left[1 + \exp\left(\frac{\varepsilon_{n-1}}{T}\right) \right] \right) \right] (k) \\
&+ \frac{1}{2c} \left[f * \left(\frac{\partial \varepsilon_{n+1} / \partial c}{1 + \exp(-\frac{\varepsilon_{n+1}}{T})} + \frac{\partial \varepsilon_{n-1} / \partial c}{1 + \exp(-\frac{\varepsilon_{n-1}}{T})} \right) \right] (k), (n \neq 1) \\
\frac{\partial \varepsilon_1(k)}{\partial c} &= \frac{T}{2c} \left[\left(\frac{\partial f}{\partial c} - \frac{f}{c} \right) * \left(\ln \left[1 + \exp\left(\frac{\varepsilon_2}{T}\right) \right] + \ln \left[1 + \exp\left(-\frac{\varepsilon}{T}\right) \right] \right) \right] (k) \\
&+ \frac{1}{2c} \left[f * \left(\frac{\partial \varepsilon_2 / \partial c}{1 + \exp(-\frac{\varepsilon_2}{T})} - \frac{\partial \varepsilon / \partial c}{1 + \exp(\frac{\varepsilon}{T})} \right) \right] (k) \\
\lim_{n \rightarrow \infty} \frac{\partial \varepsilon_n / \partial c(k)}{n} &= 0 \\
\frac{\partial \varepsilon_n^\infty}{\partial c(k)} &= 0 \tag{B3}
\end{aligned}$$

Appendix C: Covariance under the parameter c

The thermodynamics of the system depend on four parameters: (c, μ, Ω, T) . Or we can easily deduce from (3) that they are covariant under renormalisation by c , i.e.:

$$\begin{aligned}
G(c, \mu, \Omega, T) &= c^2 G\left(1, \frac{\mu}{c^2}, \frac{\Omega}{c^2}, \frac{T}{c^2}\right) \\
n_i(c, \mu, \Omega, T) &= c n_i\left(1, \frac{\mu}{c^2}, \frac{\Omega}{c^2}, \frac{T}{c^2}\right), i = 1, 2 \tag{C1}
\end{aligned}$$

This allows one to reduce our parameter space to $\{\mu, \Omega, T\}$ and put $c = 1$ by default.

-
- [1] I. Bloch, J. Dalibard, and W. Zwerger, *Rev. Mod. Phys.* **80**, 885 (2008).
 - [2] H. Moritz, T. Stöferle, M. Köhl, and T. Esslinger, *Phys. Rev. Lett.* **91**, 250402 (2003).
 - [3] B. Laburthe Tolra, K. M. O'Hara, J. H. Huckans, W. D. Phillips, S. L. Rolston, and J. V. Porto, *Phys. Rev. Lett.* **92**, 190401 (2004).
 - [4] B. Paredes, A. Widera, V. Murg, O. Mandel, S. Fölling, I. Cirac, G. V. Shlyapnikov, T. W. Hänsch, and I. Bloch, *Nature* **429**, 277 (2004).
 - [5] T. Kinoshita, T. Wenger, and D. S. Weiss, *Science* **305**, 1125 (2004).
 - [6] L. Pollet, S. M. A. Rombouts, and P. J. H. Denteneer, *Phys. Rev. Lett.* **93**, 210401 (2004).
 - [7] E. H. Lieb and W. Liniger, *Phys. Rev.* **130**, 1605 (1963).
 - [8] E. H. Lieb, *Phys. Rev.* **130**, 1616 (1963).
 - [9] A. H. van Amerongen, J. J. P. van Es, P. Wicke, K. V. Kheruntsyan, and N. J. van Druten, *Phys. Rev. Lett.* **100**, 090402 (2008).
 - [10] Y.-a. Liao, A. S. C. Rittner, T. Paprotta, W. Li, G. B. Partridge, R. G. Hulet, S. K. Baur, and E. J. Mueller, *Nature* **467**, 567 (2010).
 - [11] A. Widera, S. Trotzky, P. Cheinet, S. Fölling, F. Gerbier, I. Bloch, V. Gritsev, M. D. Lukin, and E. Demler, *Phys. Rev. Lett.* **100**, 140401 (2008).
 - [12] M. Erhard, H. Schmaljohann, J. Kronjäger, K. Bongs, and K. Sengstock, *Phys. Rev. A* **69**, 032705 (2004).
 - [13] D. M. Harber, H. J. Lewandowski, J. M. McGuirk, and E. A. Cornell, *Phys. Rev. A* **66**, 053616 (2002).
 - [14] J. M. McGuirk, D. M. Harber, H. J. Lewandowski, and E. A. Cornell, *Phys. Rev. Lett.* **91**, 150402 (2003).
 - [15] K. M. Mertes, J. W. Merrill, R. Carretero-González, D. J. Frantzeskakis, P. G. Kevrekidis, and D. S. Hall, *Phys. Rev. Lett.* **99**, 190402 (2007).
 - [16] R. P. Anderson, C. Ticknor, A. I. Sidorov, and B. V. Hall, *Phys. Rev. A* **80**, 023603 (2009).
 - [17] P. Wicke, S. Whitlock, and N. van Druten, *ArXiv e-prints* (2010), 1010.4545.
 - [18] E. Haller, M. Gustavsson, M. J. Mark, J. G. Danzl, R. Hart, G. Pupillo, and H.-C. Nägerl, *Science* **325**, 1224

- (2009).
- [19] C. Chin, R. Grimm, P. Julienne, and E. Tiesinga, *Rev. Mod. Phys.* **82**, 1225 (2010).
- [20] L. Tonks, *Phys. Rev.* **50**, 955 (1936).
- [21] M. Girardeau, *J. Math. Phys.* **1**, 516 (1960).
- [22] J. B. McGuire, *J. Math. Phys.* **5**, 622 (1964).
- [23] J. B. McGuire, *J. Math. Phys.* **6**, 432 (1965).
- [24] J. B. McGuire, *J. Math. Phys.* **7**, 123 (1966).
- [25] E. Brezin and J. Zinn-Justin, *Compt. Rend. Acad. Sci. Paris* **B263**, 670 (1966).
- [26] M. Gaudin, *Phys. Lett. A* **24**, 55 (1967).
- [27] C. N. Yang, *Phys. Rev. Lett.* **19**, 1312 (1967).
- [28] C. N. Yang, *Phys. Rev.* **168**, 1920 (1968).
- [29] B. Sutherland, *Phys. Rev. Lett.* **20**, 98 (1968).
- [30] B. Sutherland, *Beautiful Models* (World Scientific, 2004).
- [31] P. Schlottmann, *J. Phys.: Cond. Mat.* **5**, 5869 (1993).
- [32] P. Schlottmann, *J. Phys.: Cond. Mat.* **6**, 1359 (1994).
- [33] E. Eisenberg and E. H. Lieb, *Phys. Rev. Lett.* **89**, 220403 (2002).
- [34] X.-W. Guan, M. T. Batchelor, and M. Takahashi, *Phys. Rev. A* **76**, 043617 (2007).
- [35] S.-J. Gu, Y.-Q. Li, Z.-J. Ying, and X.-A. Zhao, *Int. Jour. Mod. Phys. B* **16**, 2137 (2002).
- [36] Y.-Q. Li, S.-J. Gu, Z.-J. Ying, and U. Eckern, *Europhys. Lett.* **61**, 368 (2003).
- [37] A. Kleine, C. Kollath, I. P. McCulloch, T. Giamarchi, and U. Schollwöck, *New J. Phys.* **10**, 045025 (2008).
- [38] J. N. Fuchs, D. M. Gangardt, T. Keilmann, and G. V. Shlyapnikov, *Phys. Rev. Lett.* **95**, 150402 (2005).
- [39] F. Deuretzbacher, K. Fredenhagen, D. Becker, K. Bongs, K. Sengstock, and D. Pfannkuche, *Phys. Rev. Lett.* **100**, 160405 (2008).
- [40] J.-S. Caux, A. Klauser, and J. van, den Brink, *Phys. Rev. A* **80**, 061605 (2009).
- [41] M. Olshanii, *Phys. Rev. Lett.* **81**, 938 (1998).
- [42] H. Bethe, *Z. Phys.* **71**, 205 (1931).
- [43] M. Takahashi, *Prog. Theor. Phys.* **46**, 401 (1971).
- [44] M. Takahashi, *Thermodynamics of one-dimensional solvable models* (Cambridge University Press, 1999).
- [45] C. N. Yang and C. P. Yang, *J. Math. Phys.* **10**, 1115 (1969).
- [46] K. V. Kheruntsyan, D. M. Gangardt, P. D. Drummond, and G. V. Shlyapnikov, *Phys. Rev. Lett.* **91**, 040403 (2003).
- [47] D. M. Gangardt and G. V. Shlyapnikov, *Phys. Rev. Lett.* **90**, 010401 (2003).
- [48] M. A. Cazalilla and A. F. Ho, *Phys. Rev. Lett.* **91**, 150403 (2003).
- [49] A. K. Kolezhuk, *Phys. Rev. A* **81**, 013601 (2010).
- [50] S. Takayoshi, M. Sato, and S. Furukawa, *Phys. Rev. A* **81**, 053606 (2010).
- [51] V. N. Popov, *Theoret. Math. Phys.* **30**, 222 (1977).
- [52] N. Wada, J. Taniguchi, H. Ikegami, S. Inagaki, and Y. Fukushima, *Phys. Rev. Lett.* **86**, 4322 (2001).
- [53] P. Deuar, A. G. Sykes, D. M. Gangardt, M. J. Davis, P. D. Drummond, and K. V. Kheruntsyan, *Phys. Rev. A* **79**, 043619 (2009).
- [54] A. Klumper and O. I. Patu, *ArXiv e-prints* (2011), 1103.6152.
- [55] A. M. Tsvetick and P. B. Wiegmann, *Advances in Physics* **32**, 453 (1983).